Numerical Solution of Wave Equations for the Stability of Inner Cometo-Sheath

Krishna M. Srivastava, Bruce T. Tsurutani, and Bruce E, Goldstein

(Jet Propulsion Laboratory, California Institute of Technology, 4800 Oak Grove Drive, Pasadene, CA 91 109)

Abstract

Numerical solution of the MHD wave equations for stability of the cometary sheath determined by the balance between the inward Lorentz body force and the outward ion-neutral drag force is obtained by using a two-point boundary value method, The eigenvalues and the eigenfunctions are obtained numerically by treating the cometary inner-sheath as a layer of finite thickness, bounded by the contact surface, i.e., the diamagnetic cavity boundary. The magnetic field structure discovered in the ionosphere of comets Halley and Giacobini-Zinner is found to be unstable. The effects of finite plasma pressure, dissociative recombination and mass loading due to photoionization are found to be stabilizing but are unable to quench the instability completely. It is also found that the higher the neutral production rate the lesser is the growth rate for the instability.

Subject Headings: Comets, MHD Stability

1. Introduction:

Various cometary boundaries are classified into three categories: i) cometary dynamical boundaries, ii) solar wind and IMF boundaries, and iii) transient boundaries. The dynamical boundaries are the permanent features of cometary plasma environment. The plasma in the inner coma of the comet Halley was observed by the Giotto, Vega and ICE to be almost stationary and of cometary origin. The ionosphere was detected by the magnetometer as a field free diamagnetic cavity deep within this stagnation region encountered by the Giotto (Neubauer et al., 1986). The magnetic field drops from 20 nT to nearly zero on cavity surface within a thin layer of about 25 km thickness. The magnetic field exhibits a maximum of about 50-60 nT thousands of kilometers away from the ionopause (cavity surface designated as CS) ~ 4600 kms from the nucleus. The formation of such a cavity surface can be explained by considering the balance between the inward Lorentz J X B body force and the outward ion- neutral drag force exerted on the plasma element (Cravens, 1986; Ip and Axford 1982, 1987, 1990).

The stability analysis of a thin layer of cometary plasma surrounding the cavity surface (ionosphere) is performed by taking it as an inhomogeneous plasma, density inversely proportional to the distance from the nucleus and magnetic field determined by the balance between the outward ion-neutral drag force and the inward magnetic stress. The stability analysis of the cometary ionosphere/ion opause was performed by Ershkovich et al., (1989) and Mckenzie et al., (1990) using (JWKB) approximation. Certain

limiting cases of the wave equa ions were studied under the slow variation approximation.

In this paper, we present numerical solutions of the wave equations derived in the above two papers by considering the cometary inner sheath as a layer of finite thickness bounded by the ionopause on the inner side. The equations are solved in the general case for certain realistic parameters for comets Halley and Giacobini-Zinner by using a two-point - boundary value method. The eigenvalues and the eigenfunctions are shown in figures (1)-(7). Our results indicate that the cometary sheath is linearly unstable to perturbations of certain wavelengths. The photoionization, recombination and plasma pressure have the effects of stabilizing the boundary, but the instabi ity still persists for certain wave numbers.

The paper is organized as follows: In section 2 we present the linearized non-dimensional MHD equations suitable for numerical computation as a two point boundary value problem. Computational procedure is described in section 3, and results are discussed in section 4. A summary of results and concluding remarks are given in section 5.

2. Basic Equations Governing the Stability:

2.1 The Configuration:

The magnetic field structure is derived following the Ip and Axford model which assumes that the plasma inertia and pressure are negligible. Thus, the balance between the magnetic stresses acting on the plasma element

and the ion-neutral friction determines the equilibrium structure of the magnetic field. The density is assumed to be inversely proportional to a power of the distance from the nucleus and is taken as

$$n_i = n_{io} \quad (r/L)^s \tag{1}$$

where L is some radial scale length, r is the distance from the nucleus and s is the power law index. The magnetic field is given (Ershkovich et al., (1989)) by:

$$B_\cdot / B_m = \left(\frac{2}{s+1} \left(\frac{r_m}{r} \right)^{1-a} - \frac{1-s}{1+s} \left(\frac{r_m}{r} \right)^2 \right)^{1/2}, \quad -1 < s < 1 \tag{2a}$$

$$B_{o/B_m} = \frac{r_m}{r} \left(1 + 2 \ln \left(\frac{r}{r_m} \right) \right)^{1/2}, \quad \text{for } s = -1 \tag{2b}$$

where B. and B_m denote the magentic field and the maximum magnetic field at distances r and r_m from the nucleus. The subscript O refers to background equilibrium quantities.

The magnetic field vanishes at the ionosphere at a radial distance from the nucleus

$$r_o = r_m \left(\frac{1-s}{2} \right)^{\frac{1}{1+s}}, \quad s \neq -1 \tag{3a}$$

$$r_\cdot = r_m \exp(-1/2), \quad \text{for } s = -1 \tag{3b}$$

2.2 Wave Equations for a cold plasma:

The stab lity analysis is made by taking a planar geometry. T h e equilibrium magnetic field is assumed to be directed along the z-axis and varies in the x-direction. The neutral gas flows along the x-direction, The equilibrium stress balance equation is given by:

$$\frac{1}{po}\frac{dPo}{dx} = \upsilon_o V_n - V_a^2/R \qquad (4)$$

where P. $= B_o^2 / 2\mu_o$, $V_a^2 = B_o^2 / \mu_o \rho_o$, and V_a^2 / R represents' magnetic tension, $\upsilon_o = \upsilon + \frac{\delta\rho_n}{Po}$ and V_n is the neutral gas velocity.

The equilibrium plasma density ρ_o is assumed to be determined by the photochemical equilibrium, (neglecting convection) viz.,

$$\alpha\rho_o^2 / M_i = \delta\rho_n \qquad (5)$$

where α is the dissociative recombination rate, and $\delta\rho_n$ is the photoionization rate and M_i is the ion mass of water group ions. The equilibrium density of cometary ions in the ionosphere of comet Halley is taken as 3000 cm^{-3} for an electron temperature Te ≅ 300 K, (Ip et al. 1987) $\alpha \cong 7 \times 10^{-7}$, and $\delta \cong 10^{-6}/s$

The stability analysis is restricted o twist-free perturba ions, i.e., $\underline{B}.\text{grad}\ \underline{B}$ is neglected. Following the usual procedure for the derivation of the linearized stability equations, we arrive at the following two-wave equations:

$$\left[\left(\frac{\partial}{\partial t}+\beta\right)\left(\frac{\partial}{\partial t}+\upsilon_o\right)+N^2\right]q=\frac{g}{V_a^2}\ \frac{\partial p_m}{\partial t}-\left(\frac{\partial}{\partial t}+\beta\right)\ \left(\frac{\partial}{\partial x}\ \frac{2}{R}\right)p_m \tag{6}$$

$$\left[\frac{\partial^2}{\partial y^2}-\frac{1}{V_a^2}\frac{\partial}{\partial t}\left(\frac{\partial}{\partial t}+\upsilon_o\right)\right]p_m=\left(\frac{\partial}{\partial t}+\upsilon_o\right)\left(\frac{\partial}{\partial x}-N^2\right)q \tag{7}$$

where

$$g=\upsilon V_n,\ q=\rho_o u,\ \ p_m=\frac{\overline{B}o\cdot\overline{B}}{\mu o},\ \text{and} \tag{8}$$

$$\frac{N^*}{g}=\frac{1}{\rho o}\frac{dpo}{dx}-\frac{1}{Bo}\frac{dBo}{dx},\quad \beta=\frac{aPo}{M_i} \tag{8}$$

In the above, V. = v + β/2, and pm and q are perturbations in magnetic pressure and particle flux along x.

Assuming that perturbations in all physical quantities vary as

$$Q(x,y,t)=Q(x)\exp(iky-i\omega t) \tag{9}$$

and using the following non-dimensional quantities

$$\omega^*=\frac{\omega}{\Omega_i},\ \ \tau=\Omega_i t,\ \ k^*=kL,\ \ y^*=\frac{y}{L},\ \ x^*=\frac{x}{L}$$

$$q^*=\frac{q\Omega_i L}{P_{mo}},\ \ p_m^*=\frac{P_m}{P_{mo}},\ \ V_a^{*-2}=gL/V_a^2,\ \ \upsilon_o^*=\upsilon_o/\Omega_i \tag{1o}$$

where L is a characteristic scale length, P_{m0} is equilibrium magnetic pressure and Ω_i is the ion gyration frequency, the non-dimensional forms of equations (6) and (7) dropping asterisks suitable for numerical solution can be written in the form:

$$\frac{dp_m}{dx} = \left[\frac{-i\omega}{V_a^2(\beta - i\omega)} - E^2\right] Pm \quad \left[\upsilon_o - i\omega + \frac{N^2}{\beta - i\omega}\right] q \tag{11}$$

$$\frac{dq}{dx} = \left[\frac{k^2}{\upsilon_o - i\omega} + \frac{i\omega}{gV_a^2}\right] P_m + \frac{N^2}{g} q \tag{12}$$

2.3 Wave Equations for a Warm Plasma:

The corresponding set of non-dimensional equations for a warm plasma i.e., including the plasma pressure and appropriate energy equations are (using the same non-dimensional quantities as given in (10) and dropping asterisks)

$$\left(\frac{\partial^2}{\partial t^2} + b\frac{\partial}{\partial t} + c\right)\left(\frac{\partial}{\partial t} + \upsilon_o\right) + N^2\left(\frac{\partial}{\partial t} + \beta_e\right) q$$

$$= \left[\frac{g}{Va^2}\frac{\partial}{\partial t}\left(\frac{\partial}{\partial t} + \gamma\alpha\right) - \left(\frac{\partial^2}{\partial t^2} + b\frac{\partial}{\partial t} + c\right)\frac{\partial}{\partial x}\right] p_t \tag{13}$$

$$\left[\left(\frac{\partial^2}{\partial t^2} + b\frac{\partial}{\partial t} + c\right)\frac{\partial^2}{\partial y^2} - V_p^{-2}\frac{\partial}{\partial t}\left(\frac{\partial}{\partial t} + \upsilon o\right)\left(\frac{\partial}{\partial t} + \beta\right) \bullet \left(\frac{\partial}{\partial t} + \gamma a\right)\right] p_t$$

$$= \left(\frac{\partial}{\partial t} + \upsilon_o\right)\left[\left(\frac{\partial^2}{\partial t^2} + b\frac{\partial}{\partial t} + \gamma c\right)\frac{\partial}{\partial x} - \frac{N^2}{g}\left(\frac{\partial}{\partial t} + \beta\right)\left(\frac{\partial}{\partial t} + \beta_e\right)\right] q \tag{14}$$

where

$$\beta^* = \beta / \Omega_i,\ \beta_e^* = \frac{\beta e}{\Omega_i} = \frac{\gamma\alpha}{\Omega_i} \cdot \frac{V_a^2}{V_p^2} \cdot \frac{N_m^2}{N^2},\quad \alpha^* = \frac{\alpha}{\Omega_i} = \beta^* / 2$$

$$V_p^{*2} = \left(V_a^2 + c_o^2\right) / \left(L^2\Omega_i^2\right),\ N^{*2} = N^2 / \Omega_i^2$$

$$b^* = \frac{\alpha^* + (\gamma\alpha^* + \beta^*) C_1^2}{1 + C_1^2}, \quad C_1^2 = V_a^2 / c_o^2 \tag{15a}$$

$$C^* = C_1^2 \gamma\alpha^* \beta^* / \left(1 + C_1^2\right)$$

N and N_m are the Brunt-Väisälä frequencies,

$$\frac{N^2}{g} = \frac{1}{p_o} \frac{dp_o}{dx} - \frac{1}{\rho_o V_p^2} \frac{dp_{to}}{dx}, \qquad g = \upsilon Vn, \tag{15b}$$

$$\frac{N_m^2}{g} = \frac{1}{p_o} \frac{dP_o}{dx} \cdot \frac{1}{\rho_o V_{ao}^2} \frac{dp_{go}}{dx} \tag{15c}$$

Here, Vp, is the fast magnetosonic speed and $c_o = \sqrt{\frac{\gamma p_{go}}{P_o}}$ is the sound speed.

Assuming as usual that all perturbations have the form as given in Eq. (9), we can rewrite Eqs. (13) and (14) in the following form suitable for numerical computation:

$$\frac{dp_t}{dx} = \left(i\omega + \upsilon_o + \frac{N^2(\beta e - i\omega)}{\left(\omega^2 + ib\omega - c\right)} \right) q + \frac{g}{V_p^2} \cdot \frac{\omega^2 + i\omega\alpha\gamma}{\omega^2 + ib\omega - c} p_t \tag{16}$$

$$\frac{d}{dx} q = \left[\frac{k^2}{(i\omega - \upsilon_o)} - \frac{i\omega(\beta - im)(ycx - ice)}{\left(\omega^2 + ib\omega - c\right)} \right] p_t - \frac{N^2}{g} \frac{(\beta_e - i\omega)(\beta - i\omega)}{w^2 + ib\omega - c} q \tag{17}$$

The background equilibrium quantities, viz., V_a^2, N^2, β, β_e, b, and c are calculated using the density and magnetic field distributions given in Eqs. (1) and (2b).

3. Numerical Procedure:

Equations (9), (10), and (16), (17) are solved numerically as an eigenvalue problem by using a two-point boundary value method. They are written in the form:

$$DZj - \sum_{m=1}^{2} A_{jm} Z_m = o, \; j = 1,2; \; m = 1,2 \qquad (18a)$$

$$Z_1 = p_m =, \text{ and } p_t = 0 \text{ at } x = 0, \qquad (18b)$$

$$Z_1 \rightarrow 0 \text{ as } x \rightarrow \infty \qquad (18c)$$

$x = x_c$ defines the exterior edge of the boundary layer and $p_t = p_m + p_g$, the perturbation in total pressure. A_{jm} is the coefficient matrix. Outside the boundary layer solutions of Eqs.(18) are written in the form

$$Z_j = \sum_{k=1}^{2} C_{jk} \exp(\lambda_k x), \; j = 1, 2 \qquad (19)$$

where C_{jk} is the fundamental matrix. The characteristic roots of the matrix, A_{jm} are λ_1 and -12, which are obtained numerically.

As the solutions are bounded as x $\rightarrow$ 00, the eigenvalues with positive real parts, viz., λ_1 must be discarded, thereby leaving only one linearly independent, exponentially decaying solution. The eigenvalues and the eigenfunctions are obtained with the help of a computer code (Scott and Watts, 1 977). This method of evaluating eigenvalues and eigenfunctins has been widely and successfully used (Nayfeh, 1981; Floryan and Saric,

1982, Srivastava and Dallmann, 1987 and references therein). For chosen values of ω_r and k, an estimate of ω_i is made. The known solutions at x = xc are used as the initial conditions and the integration is performed from $x = x_c$ to zero. In case the computed solution does not satisfy the boundary conditions at x = O , ω_i is incremented by using a Newton-Raphson scheme. The process is repeated until the boundary conditions at x = O are satisfied to within a specified accuracy. The eigenvalues of the adjoint problem are the same as those of the basic problem.

The boundary conditions at $x = x_c$ are obtained by writing Eqs. (18) in the form:

$$D\,Z = A_{\infty}\,Z \qquad (20)$$

where A is the matrix for x = xc and the bold letters denote matrices. The characteristic roots with positive real parts lead to growing solutions. Hence, the eigenvalues with positive real parts must be discarded, thereby leaving only one linearly decaying solution. To achieve this, we consider the general solution obtained by superposition of fundamental solutions. We write,

$$Z = C\,b \qquad (21)$$

The fundamental matrix C is a matrix containing no terms in x. Inverting system (21), we obtain

$$C^{-1}\,Z = b \qquad (22)$$

The asymptotic boundary conditions require that b = O. By reducing matrix A_∞ to a Jordan canonical form with the help of a similarity transformation $J = P^{-1} A_\infty P$, and by using the concept of adjoint system, we obtain the boundary conditions for the adjoint system as

$$S^* Z^* = 0, \quad \text{at } x = x_c \tag{23}$$

where S* consists of the last row of P^T, P is the similarity transformation matrix and P^T is its transpose.

The boundary conditions at $x = x_c$ for the basic system are

$$T Z = O \tag{24}$$

where T consists of the last row of P^{*T}, P^* is the complex conjugate of P and P^{*T} is its transpose,

4. Results with Application to Comets:

The plasma parameters chosen for numerical computations have been selected to refer to both comets Giacobini-Zinner and Halley. The physical parameters for comet G-Z are: r_m = 7600 km, and r. = 4600 km which, respectively, give distances at which the magnetic field has maximum and minimum values ($B_{max} \cong$ = 60 nT, B_{min} = O, Ip and Axford, 1990).
N_n, the number density of neutrals $\cong$ 2.2 x 10^5 cm^{-3} with the total sublimation rate Q $\cong$ $3x10^{28}$ molecule s^{-1} and $V_n \cong$ 0.9 km s^{-1} , v the ion neutral collision frequency $\cong$ 6 x 10^{-3} s^{-1}, α, the dissociative recombination

rate taking account of the dependence on ion and neutral densities is $\cong 7 \times 10^{-7}$ $(300/T_e)^{1/2}$ cm^3/s (Mendis et al., 1985) where T_e is the electron temperature. For $T_e \sim 300$ K (Ip et. al., 1987), α comes out to be 7×10^{-7} $cm^3 s^{-1}$. Assuming photochemical equilibrium Eq. (5) gives $n_{io} \sim 600$ cm^{-3} for $\delta \sim 10^{-6}/s$.

The background physical parameters corresponding to comet Halley in which the number density varies inversely as the distance from the nucleus are:
the sublimation rate $Q \cong 3 \times 10^{28}$ molecule s^{-1}, $V_n \cong 0.9$ km s^{-1}, the number density of neutrals $\cong 5.5 \times 10^6$ cm^{-3}, $\alpha = 3.8 \times 10^{-7}$ cm^3 /s for $T_e = 300$ K, and $n_{io} = 3000$ cm^{-3}. With this plasma number density, $B_m \sim 50$ nT at r = 8400 km. Thus $r_m =$ 8400 km, $r_o =$ 5095 km, $\beta H = 5x\ \beta$ of G-Z and V. = $7.5\ 10^{-3}\ s^{-1}$.

The non-dimensional background physical quantities are given by

$$\beta \cong 0.02/(x + x_o) \tag{25}$$

$$\beta Halley \cong 5X\ \beta G\text{-}Z \tag{25a}$$

$$x = \frac{r - r_o}{L}, \quad x_o = \frac{r_o}{L} \tag{26}$$

$$V_a^2 = \Omega_i^2 L^2 \cdot x_1 (x_m \cdot x_{1n} \cdot V_{a\,m}^2) \tag{27}$$

$$N^2 = g/(x_1 \cdot x_m \cdot x_{1n}) \tag{28}$$

$$x_1 = (x + x_o)/x_m, \; x_{1n} = 1 + 2 \ln x_1 \tag{29}$$

where r is the distance from the nucleus, V_{am} is the reference Alfvén velocity . $\hat{V}_a^2$ and β are shown in Figs. (1 a, b). The corresponding non-dimensional quantities accounting for pressure effects are written from Eq. (15).

Using the above parameters, we have calcu ated the eigenvalues and the eigenfunctions as described in the preceding section. Computational results show that the cold ionosphere is unstable for a range of wave numbers: - 5.5 E-3 km^{-1} to 3.2 E-3 km^{-1}. Corresponding unstable wave length range is: found to be 1100 km to 200 km. In the case of cometary sheath where pressure effects are included, he range of unstable wave numbers reduces to: 9.6 E-3 km-]- 1.014 km^{-1} The corresponding wavelength range for unstable waves is centered around 600 km which is in agreement with McKenzie et al. (1990).

Fig. (2) shows (ω_i , k) relation for $\beta = 0.02/(x+x_o)$, and β = O for comets Giacobini-Zinner and Halley (using (25a)). The top two panels of Fig. (2) show the (ω_i, k) relation for the cometo-sheath boundary at distances of 4620 km and 4650 km from the nucleus, The growth rates are larger by a factor of two for the boundary at 4620 km than for the boundary at 4650 km. This implies that deeper into the ionopause, growth rates increase sharply. The panel 3 from the top shows (ω_i, k) relation for the comet G-Z when recombination is neglected. By comparing panels 2 and 3, it can be seen that the growth rates are larger in the absence of recombination. Panel 4 shows the (ω_i, k) relation for the comet Halley. The growth rates are larger by a factor of 1.5 for the comet G-Z than the comet Halley due to its less production rate..

Figs. (3a,b) show the eigenfunctions p_{mi} and q_i (perturbations in magnetic pressure and particle flux) for certain wave numbers for the case" of cold plasma. It can be seen from Fig. (3a) that perturbation in magnetic pressure goes to zero at the ionopause boundary which is a boundary condition imposed on the system. The perturbation in magnetic pressure increases with increase in wavelength, It is obvious from Fig. (3b) that perturbation in particle flux increases towards the ionopause boundary - and is larger for perturbations of larger wavelengths.

Figs. (4a,b) show the corresponding basic quantities $1/V_a^2$, N^2 , β and β_e modified by the plasma pressure as a function of the distance in km from the ionopause cavity boundary.

Fig. (5) shows the (ω_i , k) relation for two sonic velocities, viz., $\sqrt{2}$, and $\sqrt{3}$ km/s. Curves labelled as 4 and 5 refer to the comet Halley and curves labelled as 1, 2, 3 refer to comet Giacobini-Zinner. It can be seen that growth rates for the cometo-sheath of comet Halley are smaller than the cometo-sheath of comet G-Z. Also they decrease with the increase in sound velocity.

Figs. (6a,b) and (7a,b) show the eigenfunctions $p_{m\,r}$, p_{mi} and q_r, q_i for certain wave numbers for $c_0^2 = 2$ km^2 s^{-2} ($p_{m\,r}$, p_{mi} , q_r , q_i are the real and imaginary parts of perturbations in magnetic pressure and particle flux respectively) as a function of distance from the ionopause. It is noted from Figs. (6a,b) that perturbation in magnetic pressure has oscillatory nature. It goes to zero at the inner boundary of the cometo-sheath which

is a boundary condition imposed on the system. Figs. (7a, b) show that perturbation in particle flux also has an oscillatory nature becoming maximum at the boundary.

It is found that the growth rates of linear instability decrease with increasing sound velocity. It can be seen from Figs. (2) and (5) that growth rates are larger if no recombination is accounted for, i.e. the ionosphere is destabilized as β decreases. The thickness of the ionopause transition layer - is only ~ 25 km (Neubauer, 1988). The deeper into the ionopause, the growth rates become larger due to the fact that hydromagnetic counterpart of square of the Brunt-Väisälä (Eckart, 1960) frequency, N2 (shown in Figs, (lb) and (4b)), is negative and increases sharply inside the ionopause transition ayer. The growth rates also decrease if n_{i0}, the plasma density increases. This implies that the growth rates decrease with increasing production rate of the neutrals. Also the greater the production rate the more is the number density of neutrals and the plasma and consequently β increases and growth rates decrease. The growth rates for comet Halley are found to be smaller (due to its larger production rate) than for the comet Giacobini-Zinner.

5. Conclusions:

We have investigated the stability of the cometo-sheath by numerically solving the MHD wave equations for he cometary sheath determined by the balance between the inward Lorentz body force and the outward ion-neutral drag force using a two-point boundary value method. The main conclusions of the study are:

1. The magnetic field structure resulting from the balance between the magnetic stresses and the ion-neutral drag force in the cometary ionosphere is unstable to disturbances of wavelengths from 200 km to 1100 km for a cold ionosphere and from 620 km to 650 km for a warm ionosphere. Thus perturbations of wavelengths centered around 600 km are unstable in both the cases.

2. Inclusion of plasma pressure in the stability analysis results in the stabilization of the ionosphere except for the wavelength range centered around 600 km.

3. Effects of plasma recombination and pressure are stabilizing but are unable to quench the instability completely. The finite amplitude effects also cannot quench the instability either (Ershkovich and Flammer, 1988). Since N^2, the square of Brunt-Väisälä frequency < 0 and increases sharply in the ionopause transition layer (25 km thickness), the inner cometo-sheath remains unstable.

4. It is found that the higher the neutral production rate the lesser is the growth rate for the instability. It is, therefore, conjectured that the inactive comets , say those at 2-3 A.U. from the sun where productivity of neutrals is less are likely to be more unstable.

5. The effect of plasma motion which is about a few km./sec (Balsiger et. al., 1986) and finite conductivity (Eviatar and Goldstein, 1988) play an important role in determining the stability of the cometo-sheath. We have

obtained the results for the stability of cometo-sheath including plasma motion, resistivity, and plasma pressure which will be reported shortly.

Acknowledgements:

Krishna M. Srivastava acknowledges the support of the Humboldt Foundation, Germany and the Max-Planck Institute for Aeronomy, Lindau, Germany for his stay during Nov.-Dee. 1990, during which this work was initiated. This work was completed during the period Krishna M. Srivstava held a senior Resident Research Associateship administered by the National Aeronautics and Space administration through the National Research Council. Useful discussions with Marcia Neugebauer, and Nick Omidi are thankfully acknowledge,

References:

Balsiger, H., et al. 1986, Nature, 321, 330.

Brunt, D. 1941, *in* Physical and Dynamical Meteorology (Cambridge: Cambridge University Press).

Cravens, T. E., and Korosmezey, A. 1986, Planet. Space Sci., 34,961.

Eckart, C. 1960, in Hydrodynamics of Oceans and Atmospheres (New York: Pergamon)

Ershkovich, A. I., and Flammer, K. R. 1988, Ap. J., 328, 967.

Ershkovich, A. I., et al. 1989, *Ap. J.*, 344,932.

Eviatar, A. , and Bruce, E. Goldstein 1988, J. Geophys. Res., 93,1759.

Floryan, J. M., and Saric, W. S. 1982, AIAA J. 20, 316

Ip, W.-H., and Axford, W. I. 1982, in Comets, ed. L. L. Wilkening (Tucson: University of Arizona Press), 588.

----------. 1987, Nature, 325, 418.

-------- --------. 1990, in Physics and Chemistry of Comets, ed. W. F. Huebner (Springer Verlag, Berlin),

McKenzie, J. F., et al. 1990, Ap. J., 360, 275. -

Mendis, D. A., Houbis, H. L. F., and Marconi, M. L. 1985, Fund. Cosmic Phys., 10, 1.

Nayfeh, A. H. 1981, J. Fluid Mech., 107, 441.

Neubauer, F. M., et al. 1986, Nature, 321, 352.

Scott, M. R., and Watts 1977, SIAM J. Numer. Anal., 14, 40.

Srivastava, Krishna M., and Dallmann, U. 1987, Phys. Fluids, 30, 1005

Figure Captions:

Fig. 1. shows $1/V_a^2$ as a function of distance in km from the ionopause.

Fig. 1a. shows the square of the Brunt-Väisälä frequency as a function of distance from the cavity surface.

Fig. *2.* shows growth rates normalized to Ω_i against the wave number normalized to L. The top and the second panel refer, respectively, to the ionopause at 4620, 4650. km from the nucleus. The third panel refers to - the case for zero recombination rate. The bottom panel gives growth rates · for the comet Halley. The top three panels give growth rates for the comet Giacobini-Zinner..

Fig. 3a. shows the perturbation in magnetic pressure for k= O.55, 0.6, 0.7 and 0.8 as a function of distance from the ionopause layer

Fig. 3b. shows the perturbation in particle flux for k=O.6, 0.7 and 0.8 against distance in km from the ionopause layer

Fig. 4a. shows $1/V_a^2$ and β modified by plasma pressure as functions of distance in km from the ionopause.

Fig. 4b. shows the square of the Brunt-Väisäla frequency and β_e (defined in the text) as functions of distance in km from the ionopause.

Fig. 5. shows growth rates normalized to Ω_i against the wave number normalized to L. The curves labelled 1,2,3, and 4 refer, respectively, to the comet Halley and Giacobini-Zinner for sound velocities equal to $\sqrt{2}$ and $\sqrt{3}$ km/s. The curve labelled 5 corresponds to zero recombination rate for the comet Giacobini-Zinner.

Fig. 6a. shows the real part of perturbation in magnetic pressure for k= 0.98, 0.99, 1.0 and 1.01 for sound velocity equal to $\sqrt{2}$ km/s against distance in km from the ionopause layer

Fig. 6b. shows the imaginary part of perturbation in magnetic pressure for k=O.99, 1.0, 1.01 and 1.014 for sound velocity equal to $\sqrt{2}$ km/s against distance in km from the ionopause layer

Fig. 7a. shows the real part of perturbation in the particle flux for k= O.98, 1.0 and 1.01 for sound velocity equal to $\sqrt{2}$ km/s against distance in km from the ionopause layer

Fig. 7b. shows the imaginary part of perturbation in the particle flux for k=O.98, 0.99 and 1.01 for sound velocity equal to $\sqrt{2}$ km/s against distance in km from the ionopause layer

DISTANCE FROM IONOPAUSE km
100
200
300
400
500
600
700
800
900
1000
0.0
0.4
0.8
1.2
1.6
2.0
2.4
2.8
3.2
3.6
4.0
18.0625 km^{-2}s^2/V$_a^2$

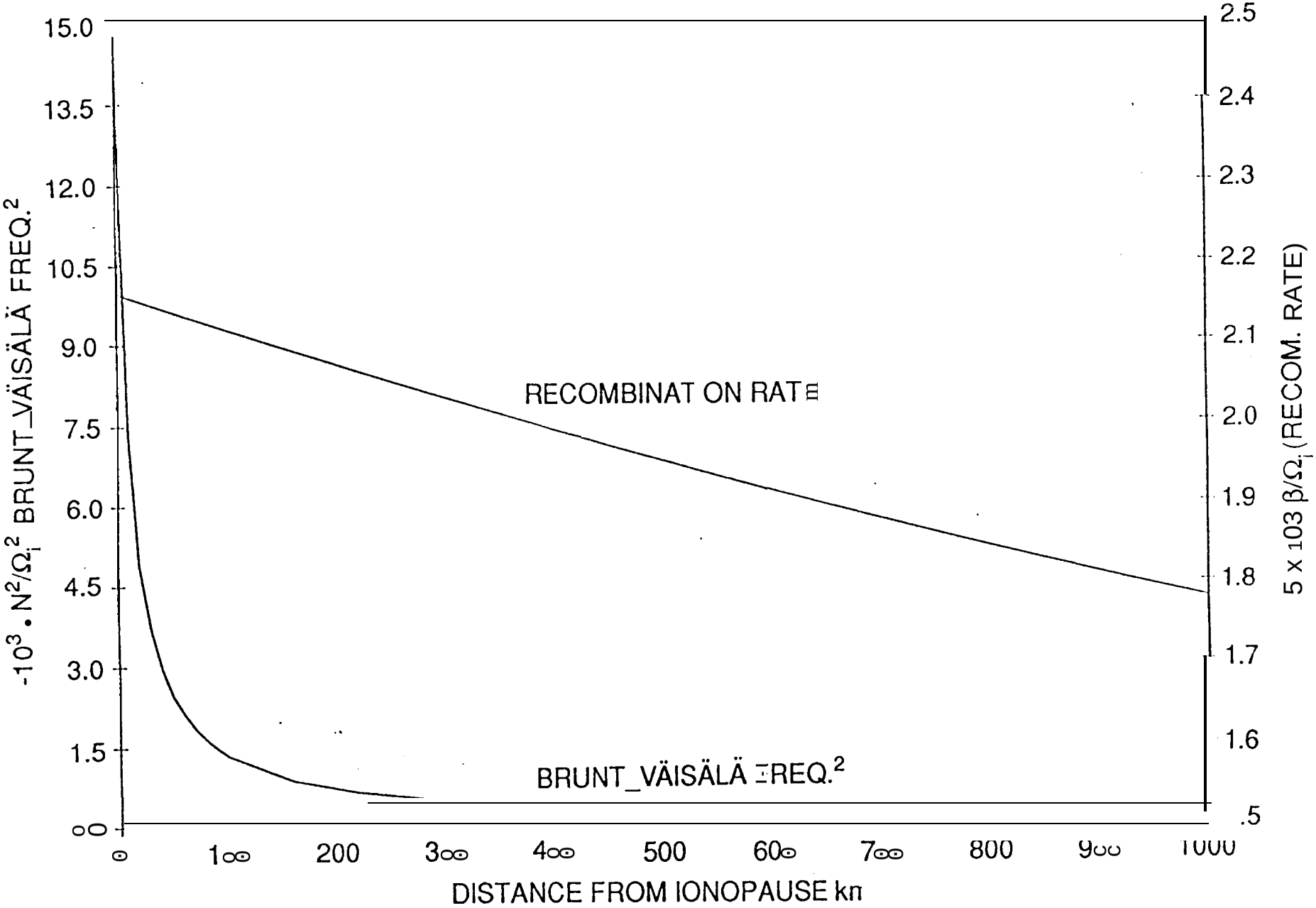
15.0
13.5
12.0
10.5
9.0
7.5
6.0
4.5
3.0
1.5
0
-10³ • N²/Ω_i² BRUNT_VÄISÄLÄ FREQ.²
2.5
2.4
2.3
2.2
2.1
2.0
1.9
1.8
1.7
1.6
.5
5 x 103 β/Ω_i (RECOM. RATE)
RECOMBINAT ON RAT
BRUNT_VÄISÄLÄ FREQ.²
0
1∞
200
3∞
4∞
500
60
7∞
800
9∞
1000
DISTANCE FROM IONOPAUSE km

FIGURE 1b

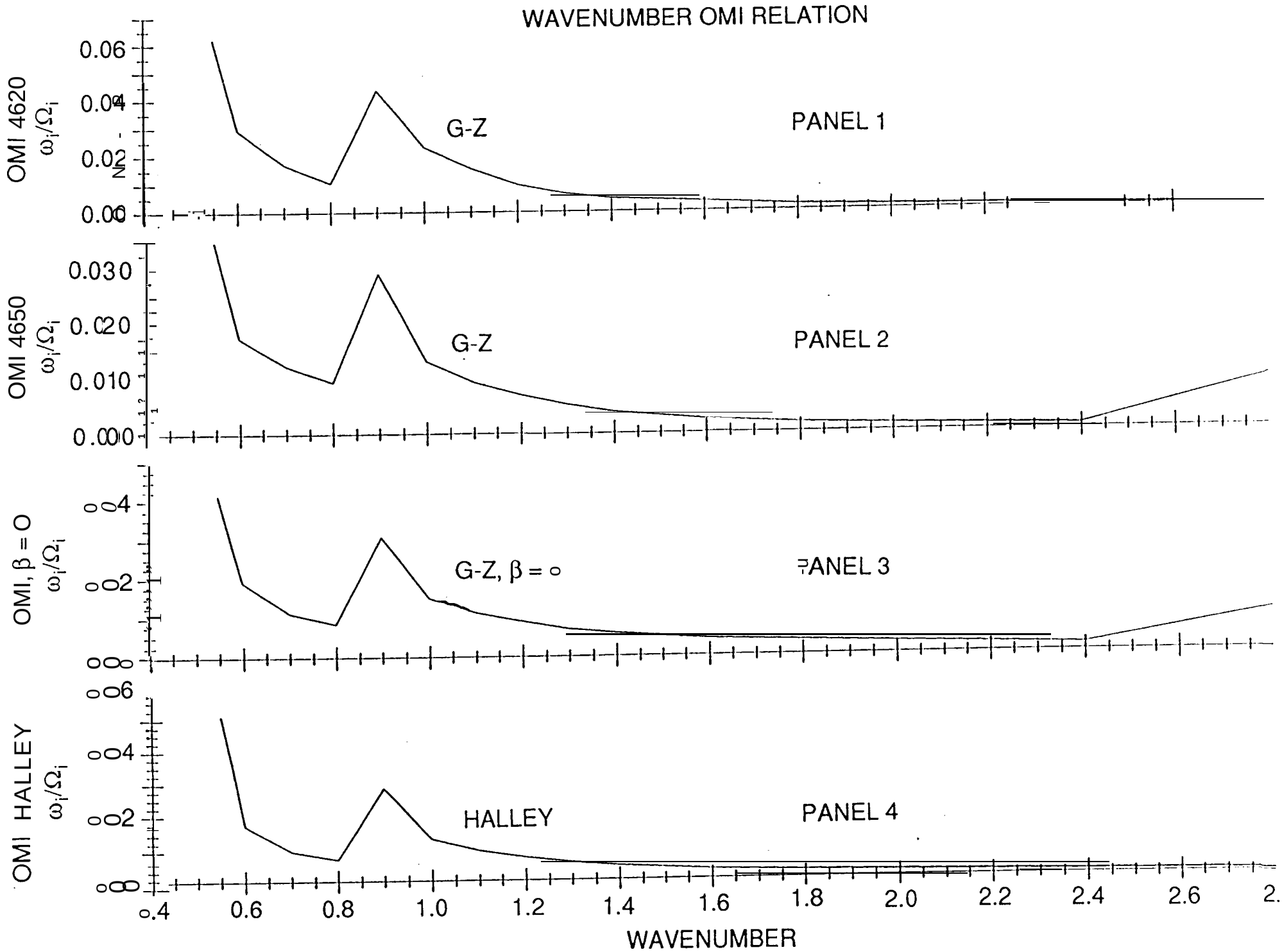
WAVENUMBER OMI RELATION
OMI 4620 ω_i/Ω_i
0.06
0.04
0.02
0.00
G-Z
PANEL 1
OMI 4650 ω_i/Ω_i
0.030
0.020
0.010
0.000
G-Z
PANEL 2
OMI, $\beta = O$ ω_i/Ω_i
G-Z, $\beta = o$
PANEL 3
OMI HALLEY ω_i/Ω_i
HALLEY
PANEL 4
0.4
0.6
0.8
1.0
1.2
1.4
1.6
1.8
2.0
2.2
2.4
2.6
WAVENUMBER

FIGURE 2

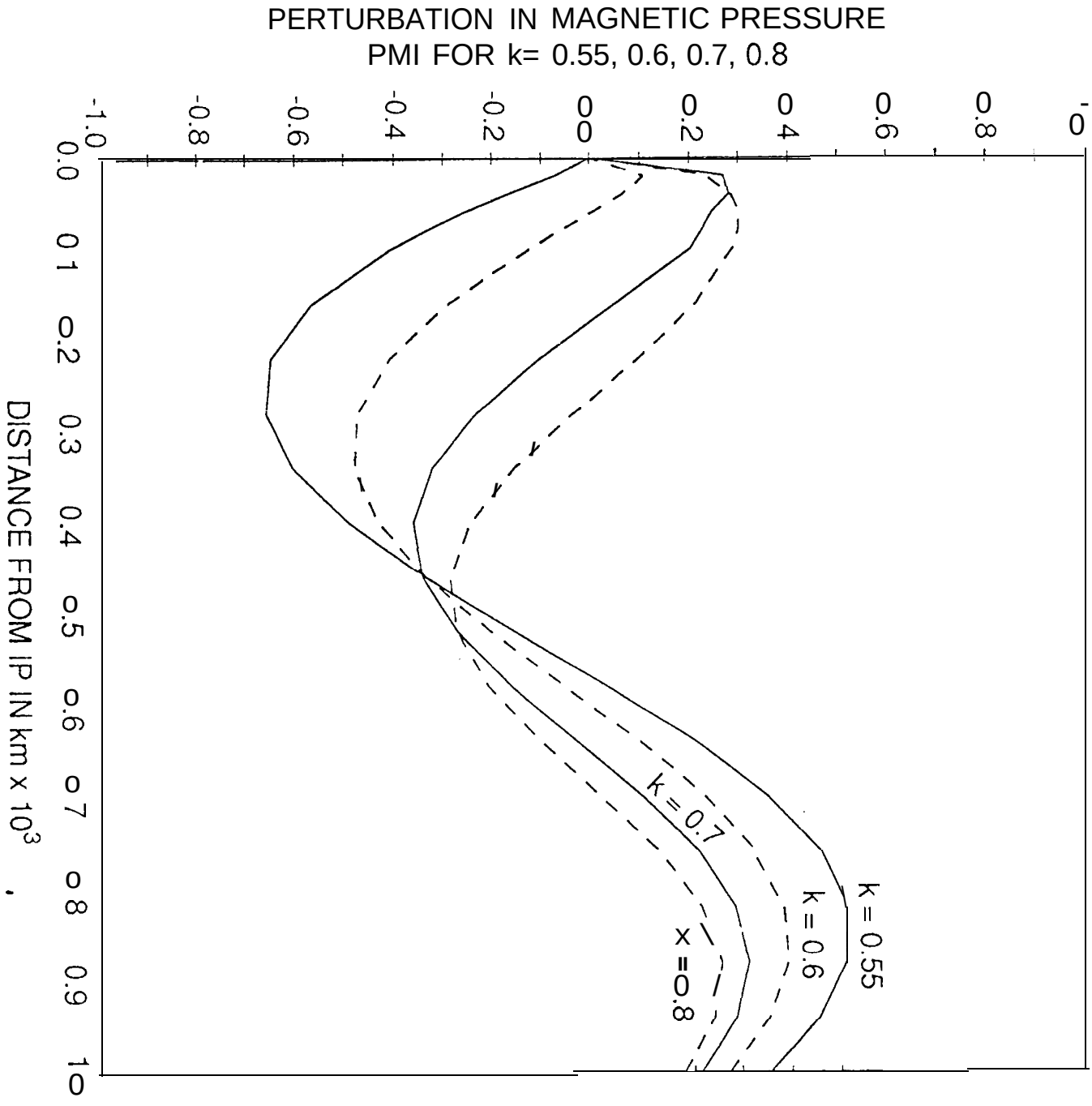
PERTURBATION IN MAGNETIC PRESSURE
PMI FOR k= 0.55, 0.6, 0.7, 0.8
-1.0
-0.8
-0.6
-0.4
-0.2
0
0.2
0.4
0.6
0.8
0.0
0.1
0.2
0.3
0.4
0.5
0.6
0.7
0.8
0.9
1.0
DISTANCE FROM IP IN km x 10^3
k = 0.55
k = 0.6
k = 0.7
x = 0.8

FIGURE 3a

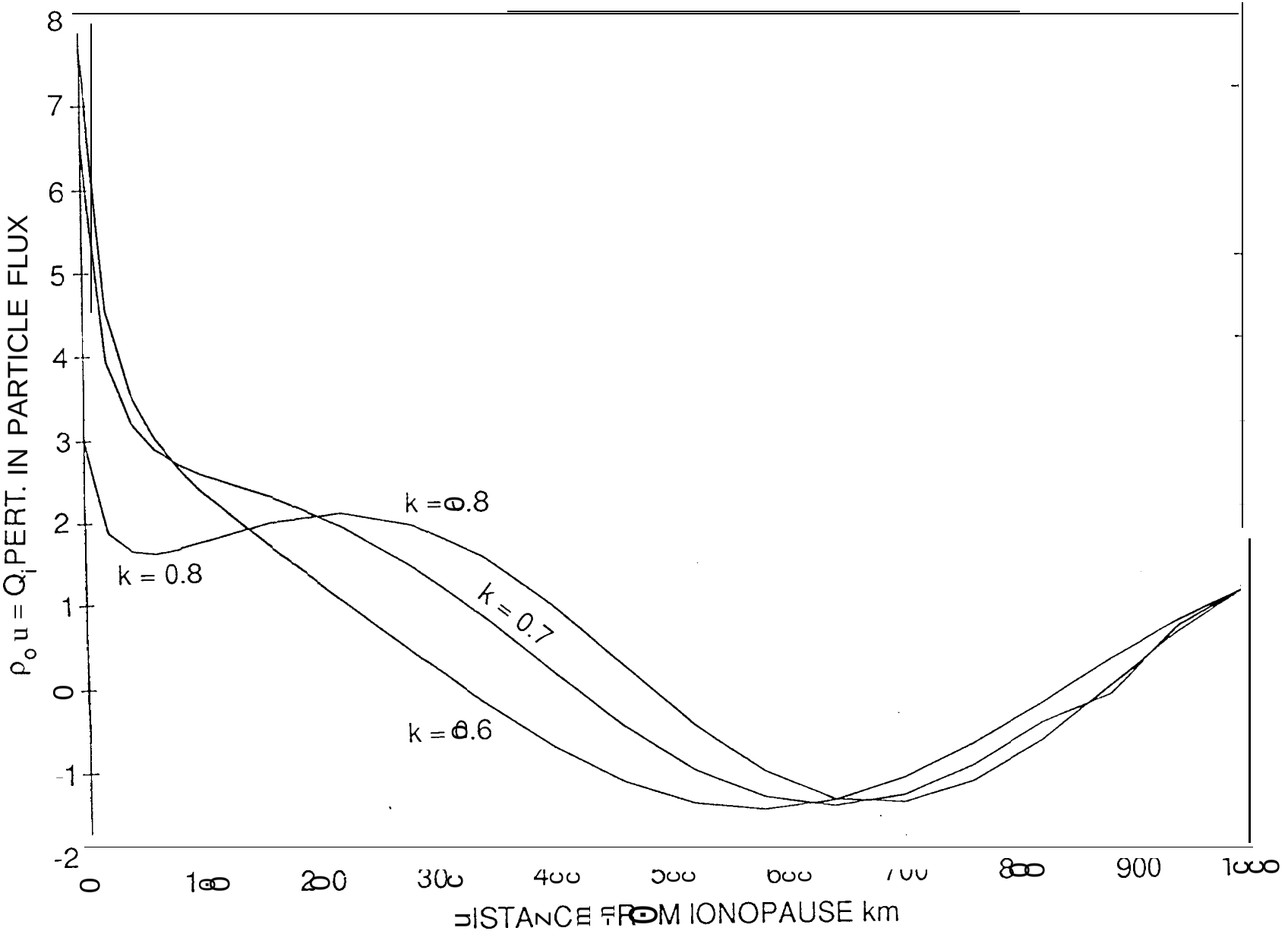
8
7
6
5
4
3
2
1
0
-1
-2
$\rho_o u = Q_i$ PERT. IN PARTICLE FLUX
k = 0.8
k = 0.8
k = 0.7
k = 0.6
0
100
200
300
400
500
600
700
800
900
1000
DISTANCE FROM IONOPAUSE km

FIGURE 36

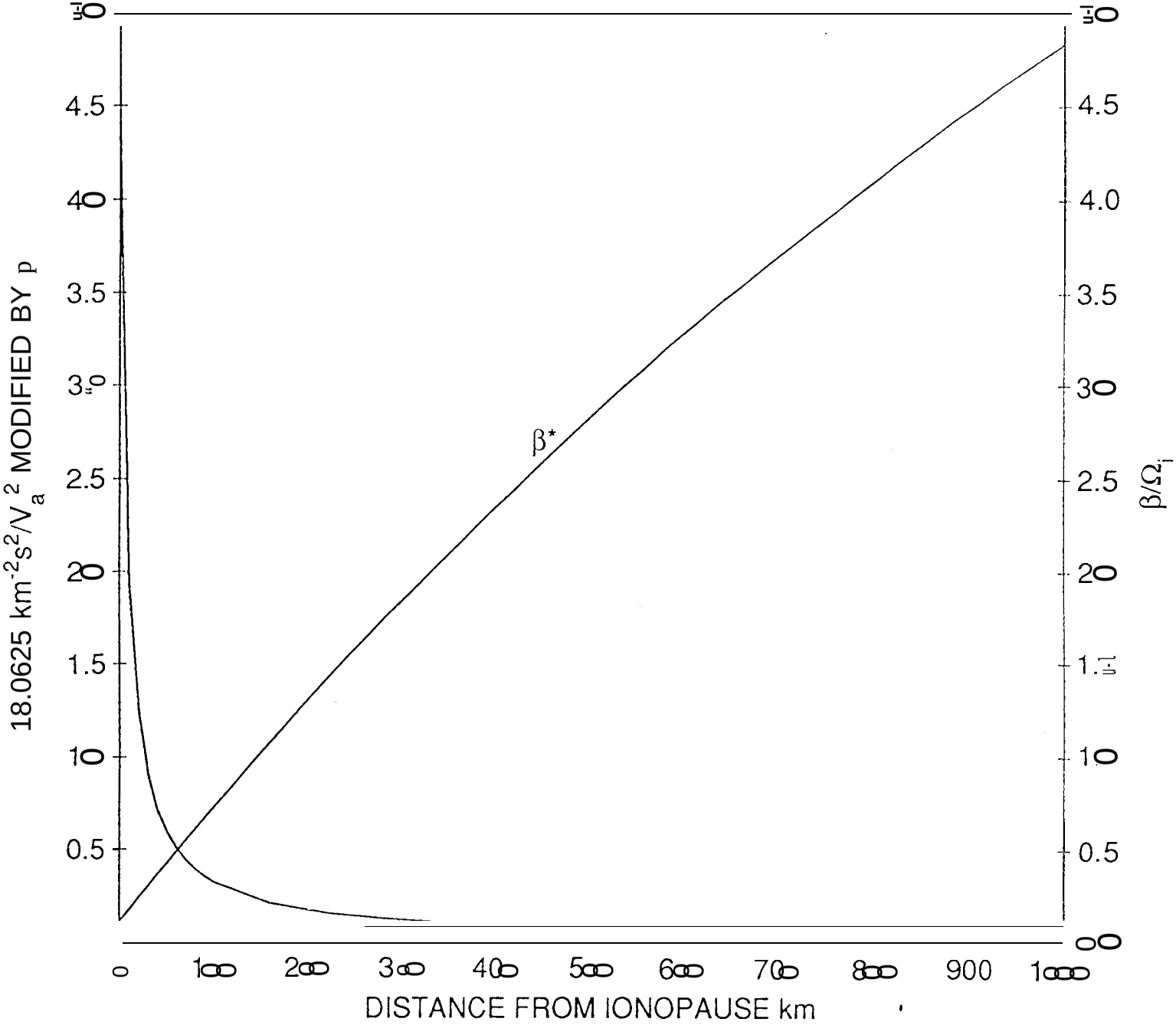
18.0625 km^{-2}s^2/V$_a$^{2} MODIFIED BY p
β*
β/Ω$_i$
DISTANCE FROM IONOPAUSE km
0
100
200
300
400
500
600
700
800
900
1000
0.5
1
1.5
2
2.5
3
3.5
4
4.5

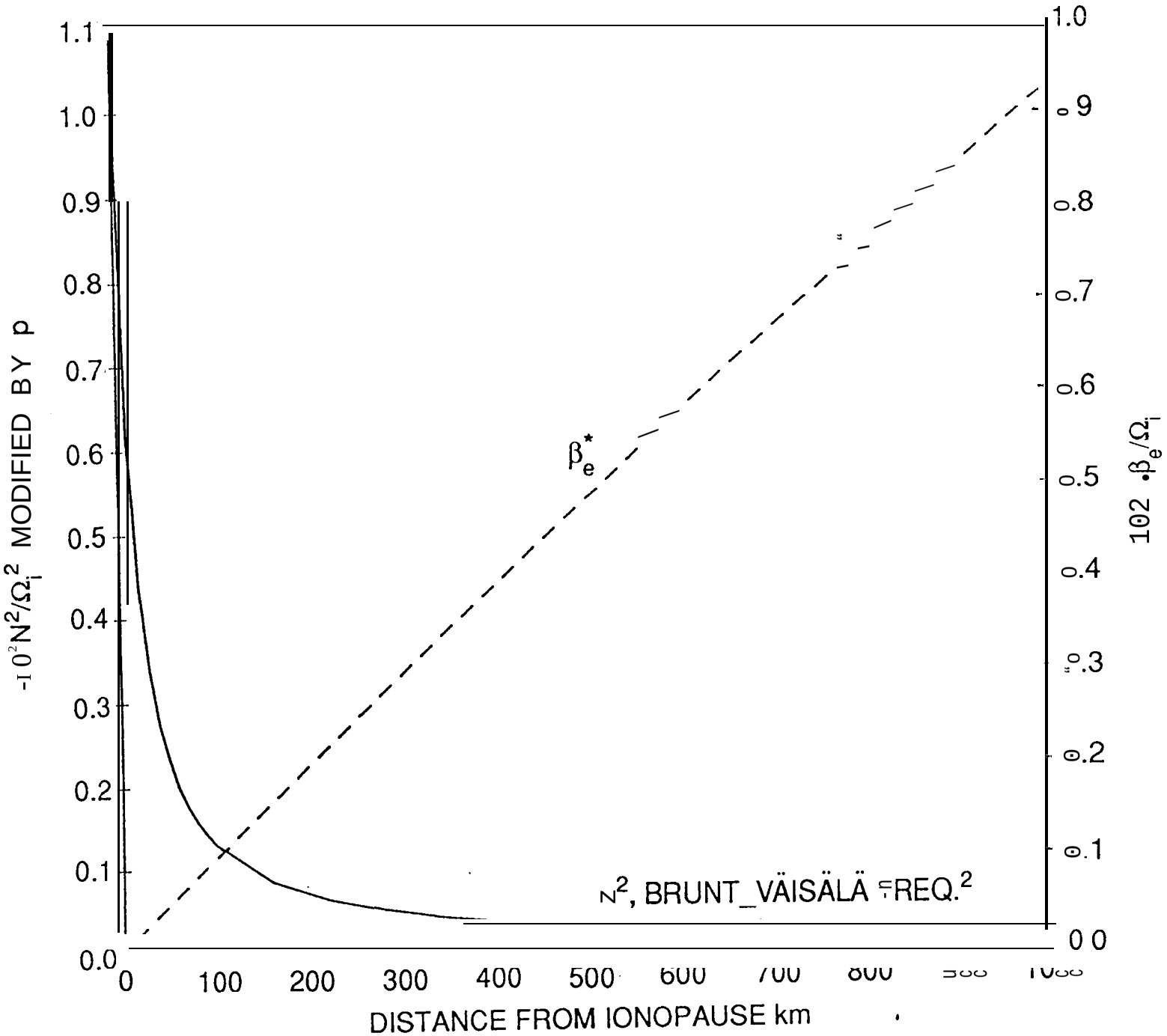
1.1
1.0
0.9
0.8
0.7
0.6
0.5
0.4
0.3
0.2
0.1
0.0
-1 0²N²/Ω_i² MODIFIED BY p
1.0
0.9
0.8
0.7
0.6
0.5
0.4
0.3
0.2
0.1
0 0
102 •β_e/Ω_i
β*_e
N², BRUNT_VÄISÄLÄ FREQ.²
0
100
200
300
400
500
600
700
800
DISTANCE FROM IONOPAUSE km

FIGURE 4b

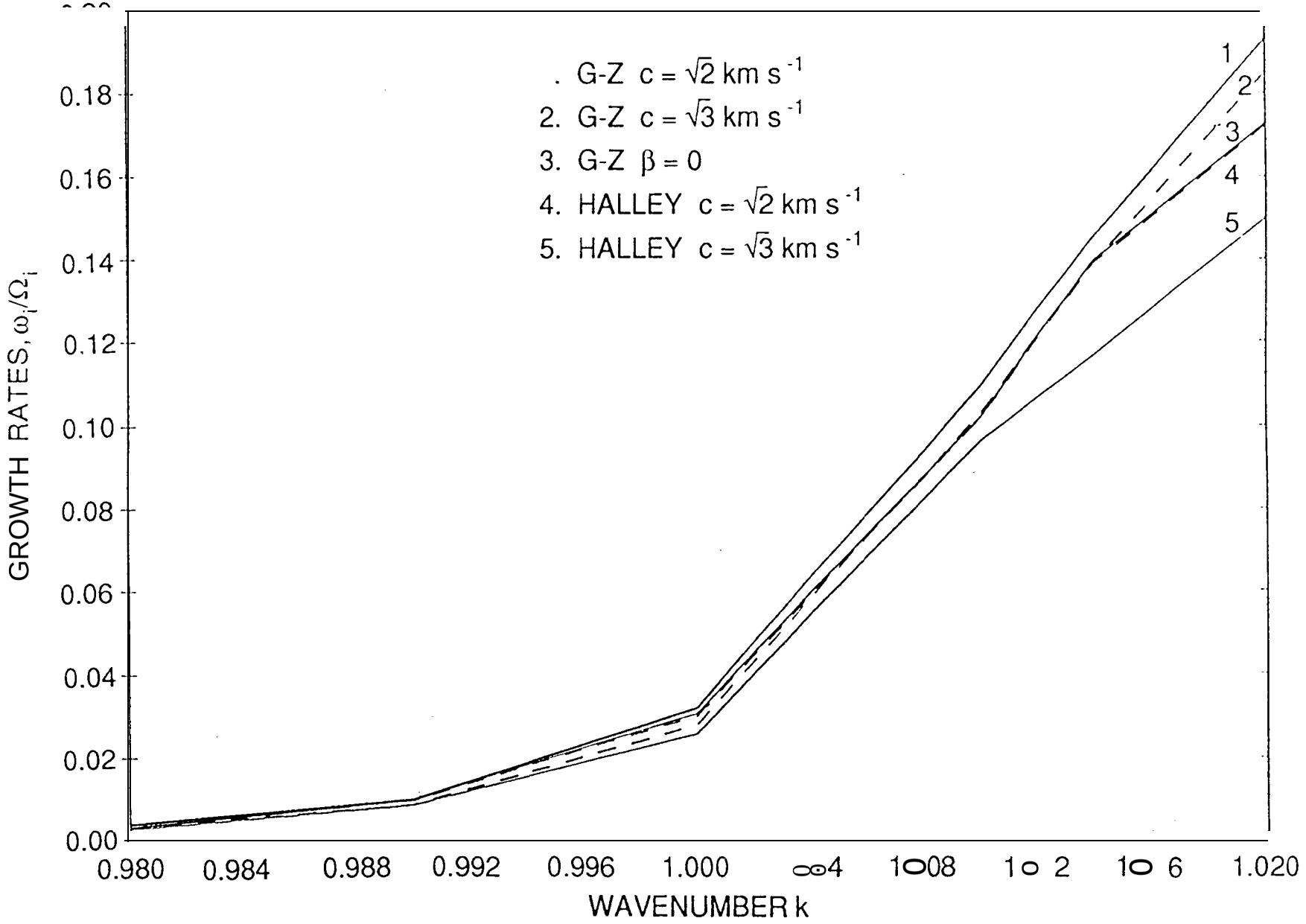
1. G-Z c = √2 km s⁻¹
2. G-Z c = √3 km s⁻¹
3. G-Z β = 0
4. HALLEY c = √2 km s⁻¹
5. HALLEY c = √3 km s⁻¹
GROWTH RATES, ω_i/Ω_i
0.00
0.02
0.04
0.06
0.08
0.10
0.12
0.14
0.16
0.18
0.980
0.984
0.988
0.992
0.996
1.000
1.004
1.008
1.012
1.016
1.020
WAVENUMBER k

FIGURE 5

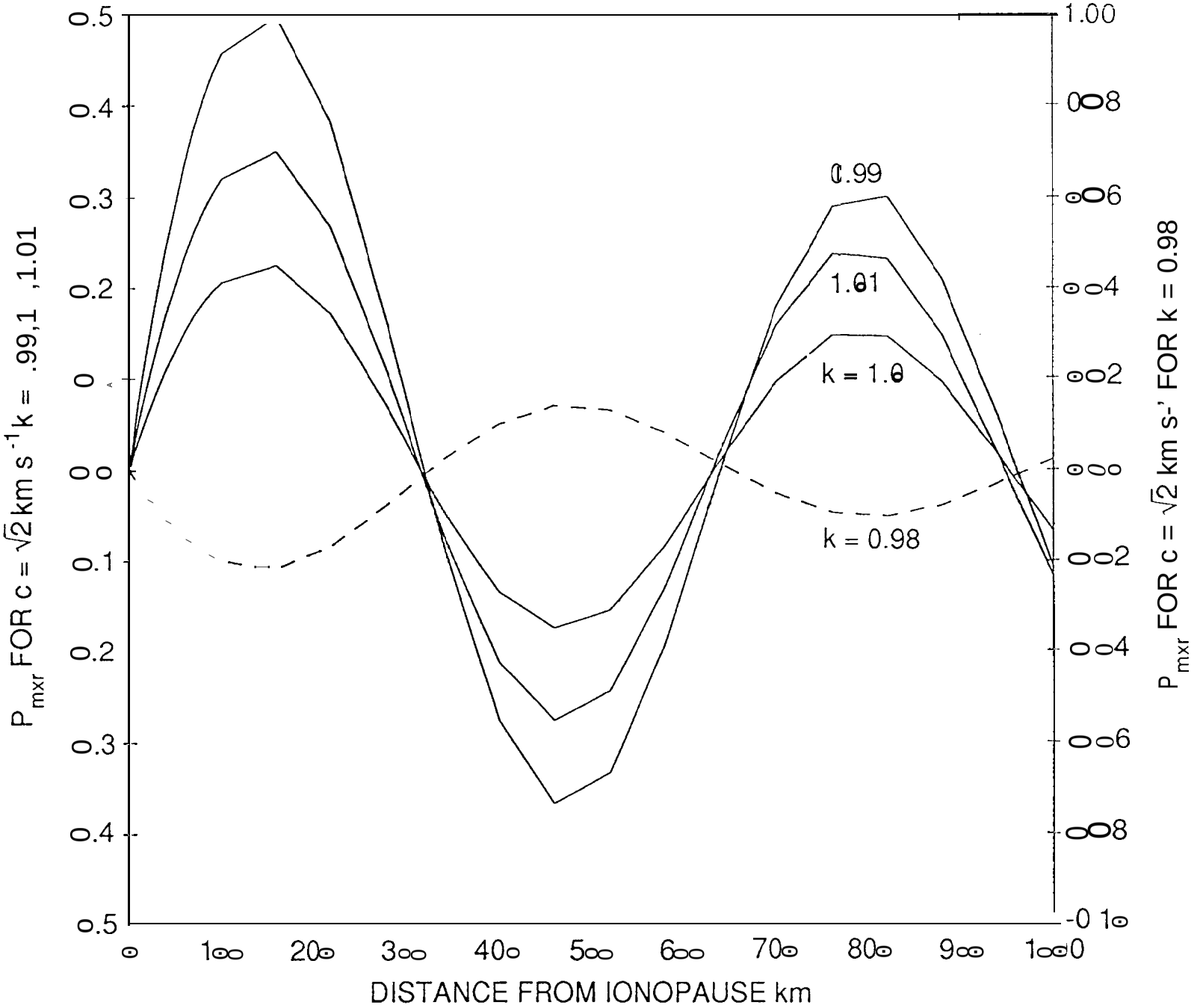
0.5
0.4
0.3
0.2
0
0
0.1
0.2
0.3
0.4
0.5
1.00
0.8
0.6
0.4
0.2
0.0
0.2
0.4
0.6
0.8
-0.1
0
1
2
3
4
5
6
7
8
9
10
0.99
1.01
k = 1.0
k = 0.98
P_{mxr} FOR c = $\sqrt{2}$ km s^{-1} k = .99,1 ,1.01
P_{mxr} FOR c = $\sqrt{2}$ km s-' FOR k = 0.98
DISTANCE FROM IONOPAUSE km

FIGURE 6a

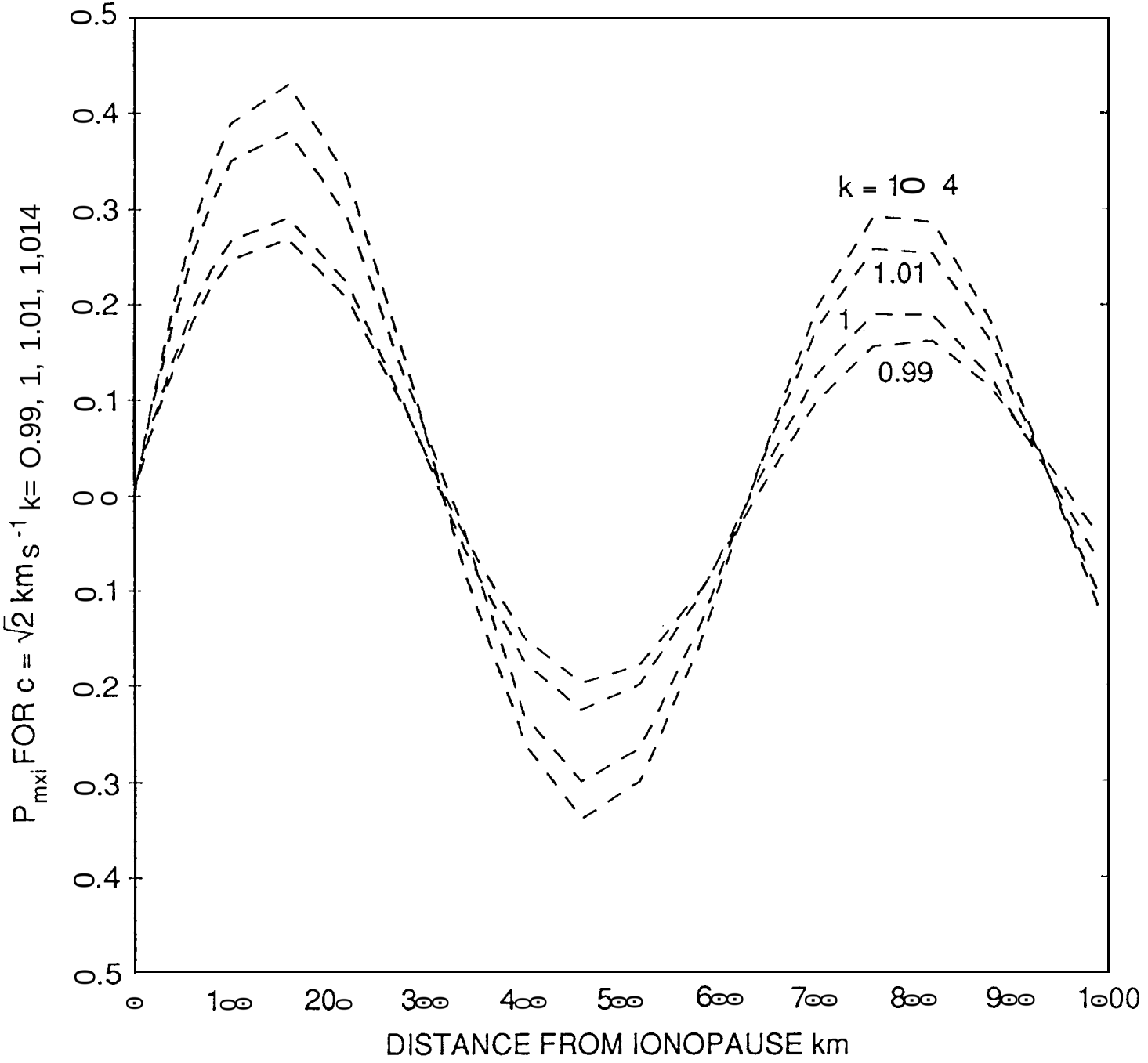
0.5
0.4
0.3
0.2
0.1
0
0.1
0.2
0.3
0.4
0.5
k = 10 4
1.01
1
0.99
0
100
200
300
400
500
600
700
800
900
1000
DISTANCE FROM IONOPAUSE km
P_mxi FOR c = √2 km s^-1 k= 0.99, 1, 1.01, 1,014

FIGURE 6b

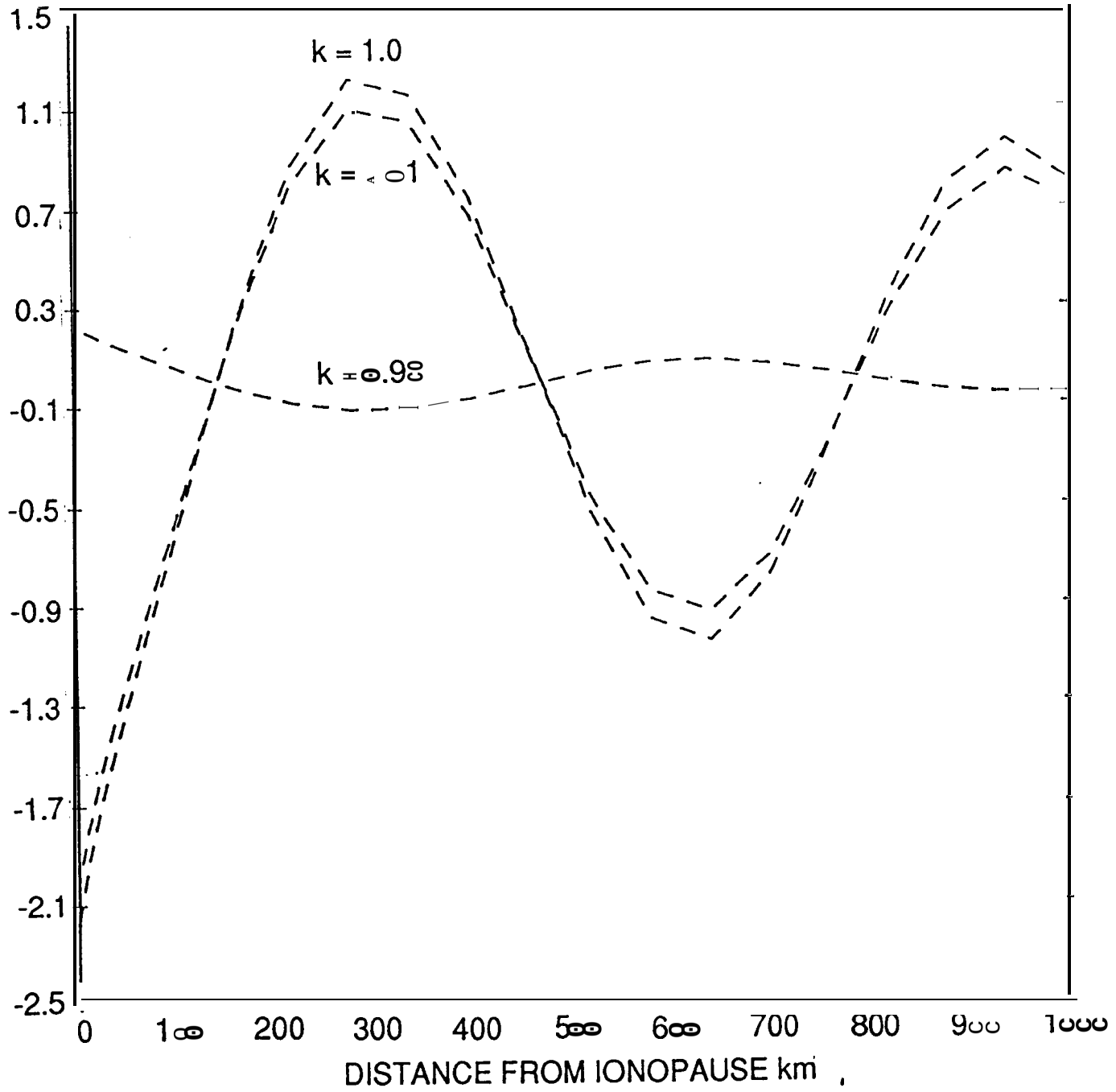
1.5
1.1
0.7
0.3
-0.1
-0.5
-0.9
-1.3
-1.7
-2.1
-2.5
k = 1.0
k = .01
k = 0.98
0
100
200
300
400
500
600
700
800
900
1000
DISTANCE FROM IONOPAUSE km

FIGURE 7a

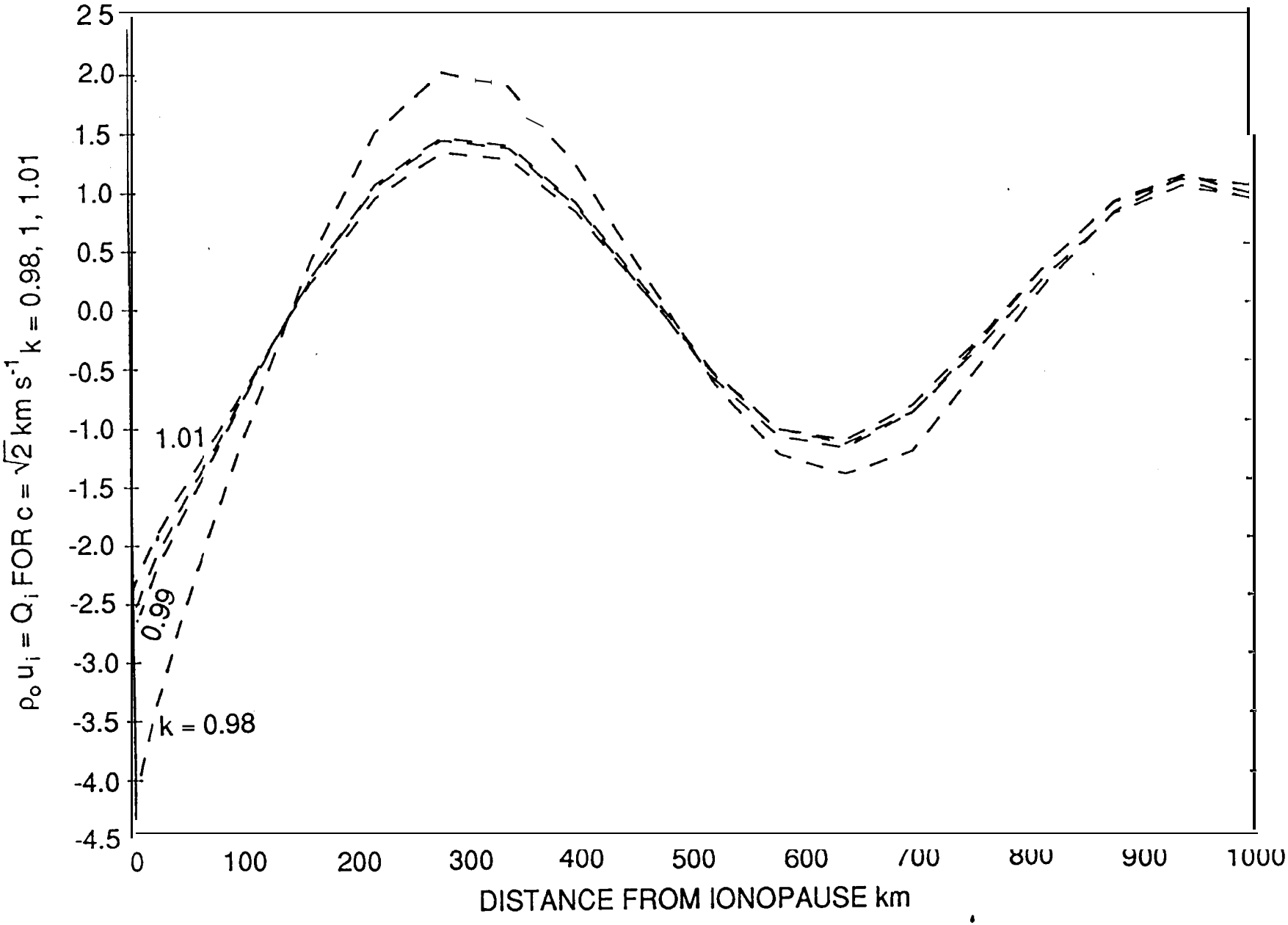
2.5
2.0
1.5
1.0
0.5
0.0
-0.5
-1.0
-1.5
-2.0
-2.5
-3.0
-3.5
-4.0
-4.5
$\rho_o u_i = Q_i$ FOR $c = \sqrt{2}$ km s^{-1} k = 0.98, 1, 1.01
1.01
0.99
k = 0.98
0
100
200
300
400
500
600
700
800
900
1000
DISTANCE FROM IONOPAUSE km

FIGURE 7b